OXFORD

Cerebral Cortex, 2014, 1–13

doi: 10.1093/cercor/bhu259
ORIGINAL ARTICLE

ORIGINAL ARTICLE

Effects of Beta-Amyloid on Resting State Functional Connectivity Within and Between Networks Reflect Known Patterns of Regional Vulnerability

Jeremy A. Elman[1], Cindee M. Madison[2], Suzanne L. Baker[1], Jacob W. Vogel[2], Shawn M. Marks[2], Sam Crowley[1], James P. O'Neil[1], and William J. Jagust[1,2]

[1]Life Sciences Division, Lawrence Berkeley National Laboratory, Berkeley, CA 94720, USA, and [2]Helen Wills Neuroscience Institute, University of California, Berkeley, CA 94720, USA

Address correspondence to Lawrence Berkeley National Laboratory, 1 Cyclotron Road Mail Stop 55R0121G, Berkeley, CA 94720-8119, USA. Email: jelman@berkeley.edu

Abstract

Beta-amyloid (Aβ) deposition is one of the hallmarks of Alzheimer's disease (AD). However, it is also present in some cognitively normal elderly adults and may represent a preclinical disease state. While AD patients exhibit disrupted functional connectivity (FC) both within and between resting-state networks, studies of preclinical cases have focused primarily on the default mode network (DMN). The extent to which Aβ-related effects occur outside of the DMN and between networks remains unclear. In the present study, we examine how within- and between-network FC are related to both global and regional Aβ deposition as measured by [^{11}C]PIB-PET in 92 cognitively normal older people. We found that within-network FC changes occurred in multiple networks, including the DMN. Changes of between-network FC were also apparent, suggesting that regions maintaining connections to multiple networks may be particularly susceptible to Aβ-induced alterations. Cortical regions showing altered FC clustered in parietal and temporal cortex, areas known to be susceptible to AD pathology. These results likely represent a mix of local network disruption, compensatory reorganization, and impaired control network function. They indicate the presence of Aβ-related dysfunction of neural systems in cognitively normal people well before these areas become hypometabolic with the onset of cognitive decline.

Key words: aging, beta-amyloid, functional connectivity, PIB-PET, resting-state fMRI

Introduction

Aggregation of β-amyloid protein (Aβ) into plaques is a characteristic neuropathological event associated with Alzheimer's disease (AD) (Braak and Braak 1991; Hardy and Selkoe 2002; Walsh and Selkoe 2004), yet many cognitively normal adults harbor significant Aβ burden at autopsy (Dickson et al. 1992; Hulette et al. 1998; Davis et al. 1999; Knopman et al. 2003; Bennett et al. 2006). With the advent of amyloid PET imaging, it is now possible to detect the fibrillar forms of Aβ in vivo (Klunk et al. 2004; Aizenstein et al. 2008). In cognitively normal older people, Aβ deposition is thought to reflect a prolonged period of preclinical pathology, eventually developing into AD (Price et al. 2009; Jack et al. 2010, 2013; Morris et al. 2010; Villemagne et al. 2013).

Aβ deposition occurs with a characteristic topography exhibiting a high degree of overlap with the DMN (Buckner 2005). Pathological processes affecting the DMN may underlie the severe memory deficits common to AD, as this region is particularly engaged during memory retrieval and periods of introspection (Raichle et al. 2001; Buckner 2004; Buckner et al. 2008). The DMN is commonly studied using resting-state functional magnetic resonance imaging (rs-fMRI) (Greicius et al. 2003; Fox et al.

2005; Damoiseaux et al. 2006). This technique may be used to identify the correlation of low-frequency fluctuations across the brain (Biswal et al. 1995), termed functional connectivity (FC), and disruptions of FC within the DMN are readily apparent in AD (Greicius et al. 2004; Seeley et al. 2009; Binnewijzend et al. 2012; Damoiseaux et al. 2012). In fact, DMN dysfunction may be utilized to differentiate AD from other neurodegenerative diseases (Seeley et al. 2009; Zhou et al. 2010). However, Aβ-related changes in FC are also found in cognitively normal subjects, despite normal memory performance (Hedden et al. 2009; Sperling et al. 2009; Sheline et al. 2010; Mormino, Smiljic, et al. 2011). These changes often consist of FC decreases in the posterior DMN but may include increases in frontal areas. While the DMN may be the primary target of AD-related change, it is not the only network affected. Studies of resting-state FC have identified a number of networks related to sensorimotor processing and higher cognitive abilities (Beckmann et al. 2005; Damoiseaux et al. 2006; Laird et al. 2011). Over the course of AD progression, changes in FC have been reported in the dorsal attention network (DAN), frontoparietal control network (FPCN), salience network (SN), and sensorimotor network (Wang et al. 2007; Zhou et al. 2010; Agosta et al. 2012; Brier et al. 2012; He et al. 2014). Whether these networks are affected during preclinical phases remains unclear.

Functional networks are composed of regions displaying largely similar patterns of activity. However, the connections maintained by these regions are not necessarily constrained by network boundaries. AD has been found to affect both local connections within networks and global links between networks (Stam et al. 2007; Supekar et al. 2008; Sanz-Arigita et al. 2010), contributing to the view of AD as a disconnection syndrome. This disconnection may occur in brain regions and hubs that are particularly vulnerable because of their high degree of connectedness and neural activity (Jagust and Mormino 2011), a hypothesis that has recently received support (Myers et al. 2014).

The long symptom-free stages of AD provide an opportunity to examine how the organization and reorganization of brain network function might antedate cognitive decline and thereby provide insight into the earliest neural alterations in AD. To explore this question, we conducted a whole-brain analysis of several functional networks measured using rs-fMRI in a group of cognitively intact older people. We employed group independent components analysis (ICA) along with a dual-regression procedure to investigate the relationship between FC and Aβ deposition, as measured by both a global index and regional Aβ. ICA is able to extract distributed sets of regions demonstrating correlated fluctuating activity, termed intrinsic connectivity networks (ICNs) (Damoiseaux et al. 2006; Beckmann 2012). This allows us to identify networks of functionally related regions in a data-driven manner for further investigation. Dual regression derives subject-specific maps of FC from the group networks, enabling us to assess comparable ICNs across subjects. These maps contain values reflecting the degree to which a voxel's time course is correlated with the mean time course of a given network. It is then possible to investigate whether the strength of these coactivations is related to another measure. This technique has been used to investigate FC changes in AD, mild cognitive impairment (MCI), and those at risk of AD (Filippini et al. 2009; Binnewijzend et al. 2012; Damoiseaux et al. 2012). By exploring the relationship between β-amyloid, measured using the PET tracer [^{11}C]PIB, and FC in a voxelwise approach, we are able to test for effects that may occur in a regionally specific manner rather than across whole networks. Employing ICA and dual regression also enables us to assess FC of a given network across the entire brain, both within its borders, and in parts of the brain that may be more strongly associated with other functional networks.

Methods

Participants

Ninety-two healthy elderly subjects underwent [^{11}C]PIB-PET and fMRI scanning (see Table 1 for subject characteristics). All elderly subjects underwent a detailed battery of neuropsychological tests described previously (Oh et al. 2014). Eligibility requirements for all subjects included no MRI or PET contraindications, living independently in the community, Mini-Mental State Examination (MMSE) ≥26, normal performance on cognitive tests (within 1.5 SD of normative values on the California Verbal Learning Test [Delis et al. 2000]) and Delayed Recall from the Visual Reproduction Test in the Wechsler Memory Scale—Third Edition (Wechsler 1997)]), absence of neurological or psychiatric illness, and lack of major medical illnesses and medications that affect cognition. Apolipoprotein E (ApoE) ε4 carrier status was determined for older subjects using previously published methods (Agosta et al. 2009). An additional 15 healthy young subjects were used as a control group to define network maps. These individuals also received [^{11}C]PIB-PET and fMRI scans. MRI scans were acquired within an average of 81.1 days of the PET. All subjects provided informed consent in accordance with the Institutional Review Boards of the University of California, Berkeley, and the Lawrence Berkeley National Laboratory (LBNL).

MRI Acquisition

Subjects were scanned in a 1.5T Magnetom Avanto (Siemens Medical Systems) scanner at LBNL. The resting-state scans were acquired with a T2*-weighted echo-planar imaging (EPI) sequence (TR = 2200 ms; TE = 50; flip angle = 90°; matrix = 64 × 64; FOV = 220 mm; 3.9 mm slice thickness). Twenty-eight axial slices oriented to the AC-PC were acquired in an interleaved order giving whole-brain coverage. One-hundred and eighty-five volumes were collected. The first 5 volumes were discarded to allow for magnetization preparation. Subjects were instructed to remain awake and keep their eyes open for the duration of the functional scan. A high-resolution T1 magnetization-prepared rapid-acquisition gradient echo (TR = 2110 ms; TE = 3.58 ms; matrix = 256 × 256; FOV = 256; sagittal plane; slice thickness = 1 mm; 160 slices) was collected for registration purposes and to determine gray matter volume.

PIB-PET Acquisition

[^{11}C]PIB was synthesized at the LBNL Biomedical Isotope Facility using a published protocol and described in detail previously

Table 1 Group characteristics

	Old	Young
N	92	15
Age	75.89 (5.6)	24 (2.8)
Gender	37 M*	8 M
Education	16.69 (2.04)	15.93 (1.53)
PIB Index	1.10 (0.19)	1.01 (0.03)
MMSE	28.93 (1.32)	28.80 (1.2)

Note: Standard deviations are listed in parentheses.
*Borderline significant relationship with PIB Index ($P = 0.055$).

(Rabinovici et al. 2007). PIB-PET imaging was performed at LBNL using an ECAT EXACT HR or BIOGRAPH Truepoint 6 scanner (Siemens Medical Systems) in 3D acquisition mode. Approximately 15 mCi of PIB was injected into an antecubital vein. Immediately upon injection, dynamic acquisition frames were obtained as follows: 4 × 15, 8 × 30, 9 × 60, 2 × 180, 10 × 300, and 2 × 600 s (90 min total). A ten-minute transmission scan or X-ray CT was obtained for attenuation correction for each PIB scan. PET data were reconstructed using an ordered subset expectation maximization algorithm with weighted attenuation. Images were smoothed with a 4-mm Gaussian kernel with scatter correction.

MRI Processing

fMRI data were preprocessed and analyzed with the FSL toolbox v5.0.4 (Smith et al. 2004). Motion correction was performed with MCFLIRT, aligning all images to the middle slice with rigid body transformation. Slice-timing correction was performed using (Hanning windowed) sinc interpolation to shift each slice in the volume in reference to the middle of the TR period. BET (brain extraction tool) was then used to create a mask of the brain from the first volume of each time series and used to separate brain from surrounding skull and tissue in each volume. All images were spatially smoothed with a 6-mm FWHM Gaussian kernel to reduce noise. High-pass temporal filtering was performed with a 100-s cutoff using the local Gaussian-weighted fit of a running line to remove low-frequency artifacts. Subject data were registered to standard space in a two-step process using FNIRT (FMRIB's Non-Linear Image Registration Tool). First, EPIs were linearly registered to each subject's skull-stripped in-plane anatomical image. Second, subject's T1-weighted images were nonlinearly registered to standard space (FSL's MNI152 template). The 2 registrations were then combined to take the subject's EPI images into standard space in 1 transformation.

Gray matter partial volume maps were included as voxelwise regressors controlling for atrophy. First, the amount of smoothing required to match that of each subject's anatomical T1 image to their functional image in standard space was estimated. Next, anatomical images were segmented into gray matter, white matter, and cerebro-spinal fluid using FSL's FAST tool. The estimated smoothing was then applied to the gray matter partial volume maps, and these images were registered to standard space for inclusion as subject-specific voxelwise regressors in the group analysis. Additionally, a group-specific probabilistic atlas (of all older subjects) was generated containing the average amount of gray matter in each voxel.

PIB-PET Processing

All PIB-PET data were preprocessed using SPM8 software (Friston et al. 2006). The first 5 frames were summed, and all frames including the summed image were realigned to the middle frame (17th frame). The subject's T1 MRI data were coregistered to their PIB-PET data using the mean image of frames corresponding to the first 20 min of acquisition as a target. PIB distribution volume ratio (DVR) images were created using Logan graphical analysis with frames corresponding to 35- to 90-min post-injection and a gray matter cerebellum reference region defined using FreeSurfer v5.1 software (Logan et al. 1996; Dale et al. 1999; Price et al. 2005). Mean DVR values from frontal, parietal, temporal, and cingulate cortices were computed to serve as a global PIB Index for all older subjects.

DVR maps were also used on a voxelwise basis to investigate effects related to regional PIB binding. Each subject's DVR image was coregistered to the structural MRI image using the inverse of the transform described earlier. The non-linear transform between each subject's structural MRI and the MNI template was then applied to move the DVR image into standard space. The smoothing of these maps was matched to that of the functional epi images after registration to standard space.

Sixty-three of the older subjects were scanned on the ECAT HR and 29 on the Biograph; the mean and standard deviations for the global PIB DVRs were almost identical (Ecat: mean = 1.10, SD = 0.19; Biograph: mean = 1.09, SD = 0.17).

Group-Independent Component Analysis and Dual Regression

Group spatial ICA was carried out with FSL's MELODIC (see Fig. 1 for summary of procedure). Registered functional data from the young control subjects were temporally concatenated and decomposed into 30 independent components (ICs). This number of components was chosen as it provides a good separation of our ICNs of interest without decomposing networks into a large number of individual regions (Abou-Elseoud et al. 2010). We chose to use only young subjects in the group ICA as they provide an independent dataset and were found to produce more robust functional networks (Rytty et al. 2013). Fourteen ICs were identified as anatomically and functionally plausible ICNs. Seven networks of interest were chosen for further analysis based on AD-related changes found in previous studies, including: classic DMN, precuneus/DMN, DAN, anterior–ventral SN, posterior–dorsal SN, left FPCN, and right FPCN. Networks were identified with a template-matching procedure against a set of previously defined network maps (Greicius et al. 2004; Shirer et al. 2012). Goodness of fit for each template network was calculated by subtracting the mean z-score of each IC falling outside of the template from the mean z-score within the template. The IC with the highest goodness of fit score with each network of interest was chosen for subsequent analysis.

Individual subject IC maps corresponding to the group networks were derived for between-subject comparisons using a dual-regression procedure (Beckmann et al. 2009; Filippini et al. 2009). First, all group IC spatial maps were entered as regressors in a linear regression against each subject's preprocessed 4D functional dataset (spatial regression). This step resulted in a set of subject-specific time courses for each group spatial map, reflecting the mean time course of each component. These time courses were then variance normalized to test for differences in IC spatial extent and amplitude. Next, these time courses were entered as regressors against the same 4D functional datasets (temporal regression) to produce a set of subject-specific spatial maps corresponding to each group IC. The value of each voxel in these spatial maps represents the degree to which it is correlated with a given network's mean time course. By including all 30 ICs in both stages of dual regression, the resulting time courses and spatial maps are partial regression estimates in which shared variance with other components (both physiologically plausible and artifactually related) is controlled.

Group Analysis of Functional Connectivity

Group analysis of older subjects was conducted with the Robust Biological Parametric Mapping (rBPM) toolbox (Casanova et al. 2007; Yang et al. 2011). rBPM allows for the inclusion of voxelwise regressors and implements a robust regression model (using the bisquare weight function) to reduce sensitivity to outliers and heteroscedasticity. Global effects of Aβ were examined by

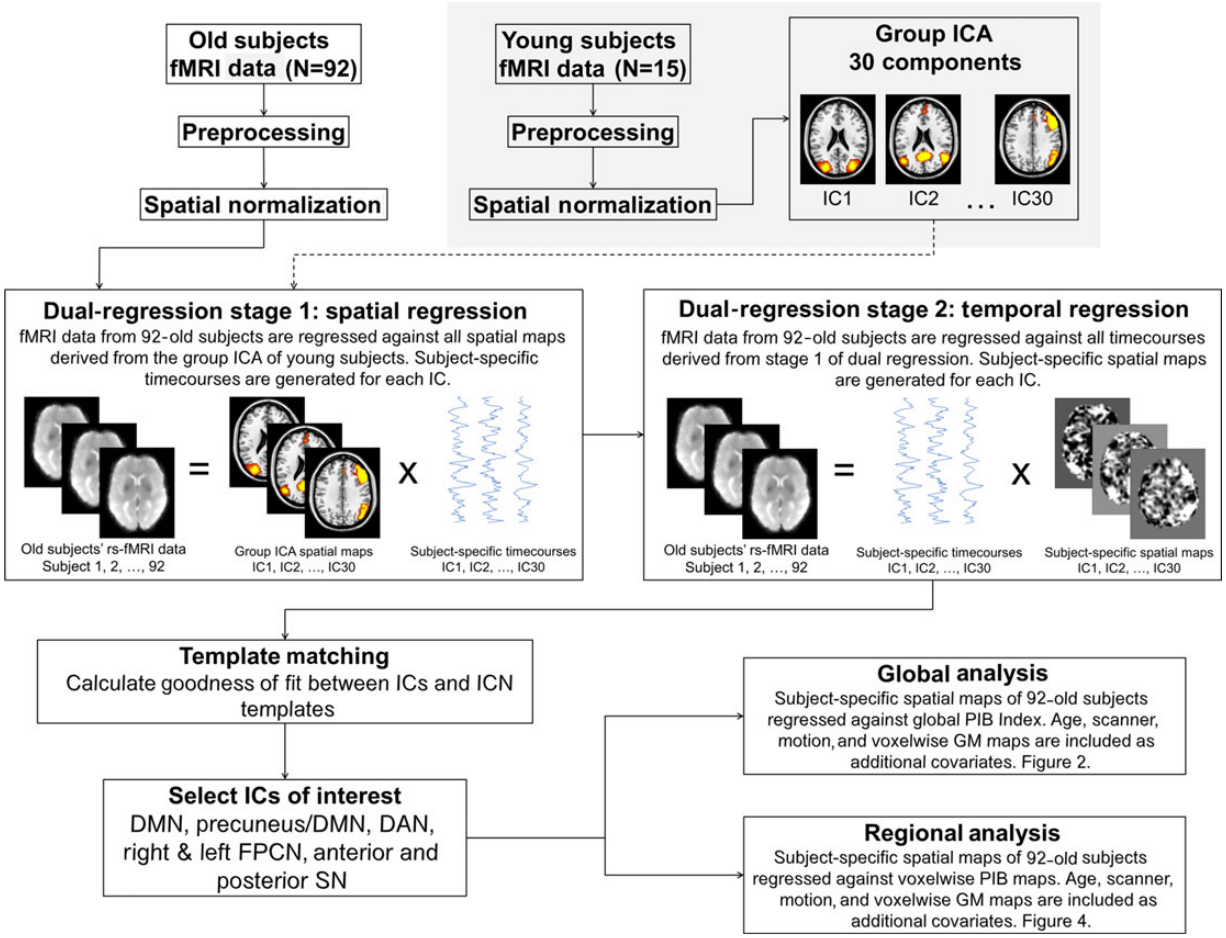

Figure 1. Flow chart of analysis. After preprocessing, fMRI data from 15 young subjects were included in a group ICA and 30 components were generated. A dual-regression procedure was employed to generate subject-specific time courses and spatial maps of each component for 92 older subjects. The first stage produces a mean network time course for each component, and the second stage produces spatial maps in which voxel values represent the degree to which that voxel's time course is correlated with the mean network time course. A template-matching procedure was used to identify 7 networks of interest for subsequent group analysis. Changes of network connectivity were tested against both global and regional measures of Aβ deposition.

regressing subject spatial maps of the 7 ICNs against each subject's PIB Index. Regional effects of Aβ were assessed by regressing ICN maps against each subject's voxelwise map of PIB DVR values. Global and regional PIB values were treated as continuous variables. Partial volume gray matter was included as a voxelwise covariate to control for regional atrophy in both analyses. The mean relative RMS deviation was included as a motion regressor, and there was no significant relationship between this measure and PIB Index [$t_{(90)} = -0.71$, $P = 0.48$]. Age and scanner were included as additional nuisance covariates. PIB Index, DVR maps, and age were log-transformed to produce a more normal distribution of values. These analyses were restricted to voxels containing at least 20% gray matter as determined by the group-specific probabilistic atlas generated by FAST. The whole-brain family-wise error was cluster-corrected to $P < 0.05$ using a voxel threshold of $P < 0.01$.

The entire brain was examined for relationships between PIB (using PIB Index or voxelwise DVR values) and each voxel's connectivity to a given network. Some of the examined brain voxels clearly fell well within the ICN that was being tested. However, other voxels fell in regions outside of the tested network in regions that were more strongly associated with a different ICN. We refer to these clusters as indicating between-network changes. To give a sense of the functional parcellation of the cortex, we created a map in which voxels are labeled according to the ICN their time course was most typical of. Labels were assigned by taking the group IC (of the 7 chosen for analysis) with the highest z-score for each voxel. These labels are presented as color overlays over which significant clusters are displayed in the results figures. ICN label maps and thresholded statistical maps were projected onto inflated atlases for display purposes using Caret v5.64 software (Van Essen 2005).

Results

Group Characteristics

Demographics for old and young subjects are listed in Table 1. There was a borderline significant difference in global PIB Index between males (mean = 1.06) and females (mean = 1.13) [$t_{(90)} = 1.944$, $P = 0.055$]. Among older subjects, global PIB Index was not significantly related to age, MMSE, years of education, or motion.

Global PIB Results

The global PIB analysis investigated changes of FC related to overall Aβ burden as measured by the PIB Index (Fig. 2 and Table 2). As

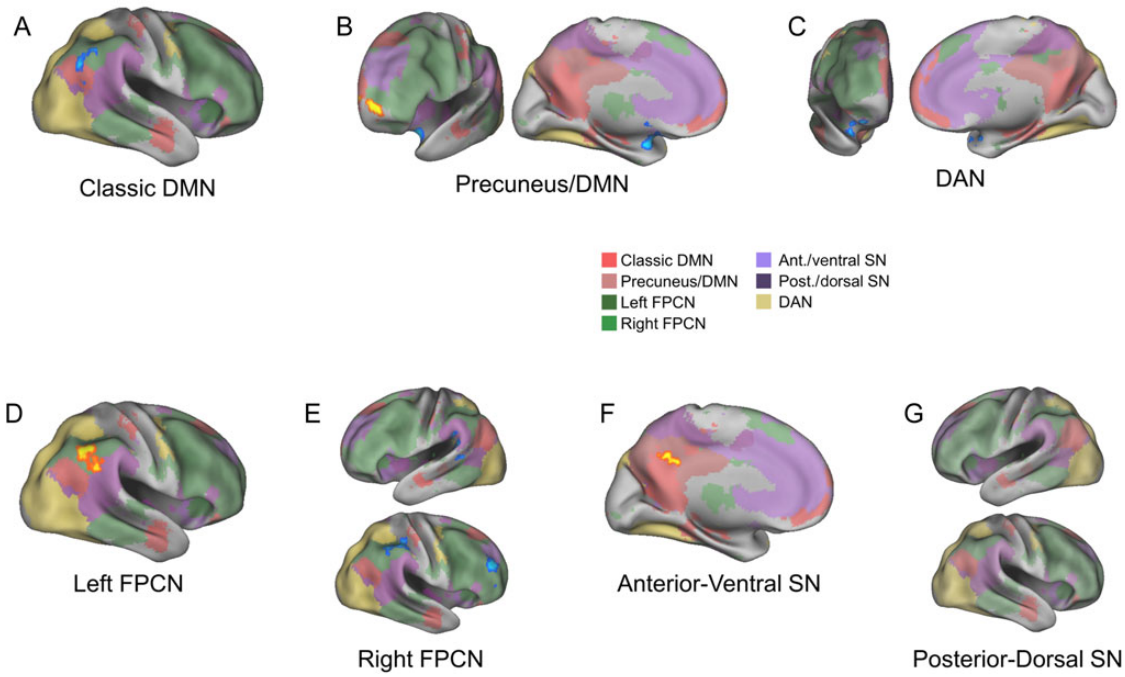

Figure 2. Global PIB results. Networks showing significant changes in FC related to PIB Index are displayed on inflated surfaces. PIB Index was derived from the mean DVR value across an averaged group of ROIs. Statistical maps representing how strongly each voxel's time course was associated with the mean time course of a given network were regressed against PIB Index using a robust regression with the bisquare weight function. Regressors controlling for age, scanner, motion, and voxelwise gray matter were included. Results were cluster-corrected to $P < 0.05$ using a voxel threshold of $P < 0.01$. Each panel displays Aβ-related changes in FC related to a different network time course (identified by the label under each set of brains). Warm colors indicate a positive relationship between PIB Index and the degree of coactivation with the mean network time course; cool colors indicate a negative relationship. See the text for information on directionality relative to baseline. The overlay colors on the brain show the group component with the highest z-score for each voxel to demonstrate the network most strongly associated with each region.

Table 2 Local maxima of global PIB analysis

Region	Hemisphere	Within/outside network[a]	X (mm)	Y (mm)	Z (mm)	z-score
Classic DMN						
Angular gyrus	R	W,O	48	−50	34	−4.44
Precuneus/DMN						
Frontal pole	L	O	−26	62	−4	3.66
Frontal orbital Cortex	L	O	−18	8	−18	−5.36
DAN						
Frontal orbital cortex	R	O	26	26	−20	−3.49
Left FPCN						
Angular gyrus	R	O	48	−50	44	5.16
Right FPCN						
Postcentral gyrus	R	W	50	−28	52	−4.65
Parietal operculum	L	O	−54	−38	24	−3.85
Frontal pole	R	W	38	44	24	−3.87
Anterior–ventral salience network						
Precuneus	L	O	−14	−54	36	7.28

Note: Regions demonstrating changes in FC related to PIB Index are listed for each network. Coordinates of local maxima within significant clusters ($P < 0.05$, cluster-corrected) are reported in MNI-space, and regional labels were derived from the Harvard-Oxford Cortical Atlas. The location of significant clusters is indicated as within or outside a tested network, corresponding to within- or between-network changes of FC, respectively.
[a]W = cluster located within tested network; O = cluster located outside tested network.

global PIB increased, a portion of the classic DMN centered in the right inferior parietal lobule (IPL) showed decreasing FC with the mean network time course (Fig. 2A). This cluster also extended into areas more associated with the right FPCN IC, indicating a potential decrease in between-network connectivity as well. The left frontal pole, which maintains a time course more typical of the left FPCN, became more strongly connected to the precuneus/DMN component with higher PIB (Fig. 2B). However, a cluster falling within the left orbitofrontal cortex (OFC) and the left temporal pole (both with time courses typical of the anterior–

ventral SN) showed less FC with the precuneus/DMN as PIB increased. There were also between-network changes associated with the DAN component. A portion of the right OFC often associated with the anterior–ventral SN showed FC decreases with the DAN (Fig. 2C). As evidenced by their decomposition into separate ICs, the left and right FPCN maintain separate connectivity profiles and are not necessarily highly correlated with each other. We found that as global PIB increased, the right supramarginal gyrus (SMG), a central node of the right FPCN, showed higher FC with the left FPCN time course (Fig. 2D). In examining FC with the right FPCN mean time course, we found multiple areas of PIB-related decreases across the brain (Fig. 2E). These included the right intraparietal sulcus and prefrontal cortex (PFC) (both coactive with the right FPCN, thus representing within-network losses of FC), and the left temporoparietal junction (TPJ), which is more closely related to the posterior–dorsal SN, representing between-network changes. Increased FC with the anterior–ventral SN was apparent in the precuneus, a region strongly associated with the DMN (Fig. 2F).

Alterations in FC were driven by both increases and decreases relative to baseline (see Fig. 3 for examples). In many cases, increased FC related to PIB reflected stronger FC in individuals with a large amount of Aβ aggregation, whereas decreases represented weaker FC. However, apparent PIB-related increases in FC may be driven by a "decrease" in anti-correlation. Conversely, PIB-related decreases in FC may actually reflect an "increase" in anti-correlation (this latter pattern did not occur in the global analysis but did occur in the regional analysis). Examples of these instances are presented in Figure 3. As previously mentioned, the right and left FPCNs may have different patterns of

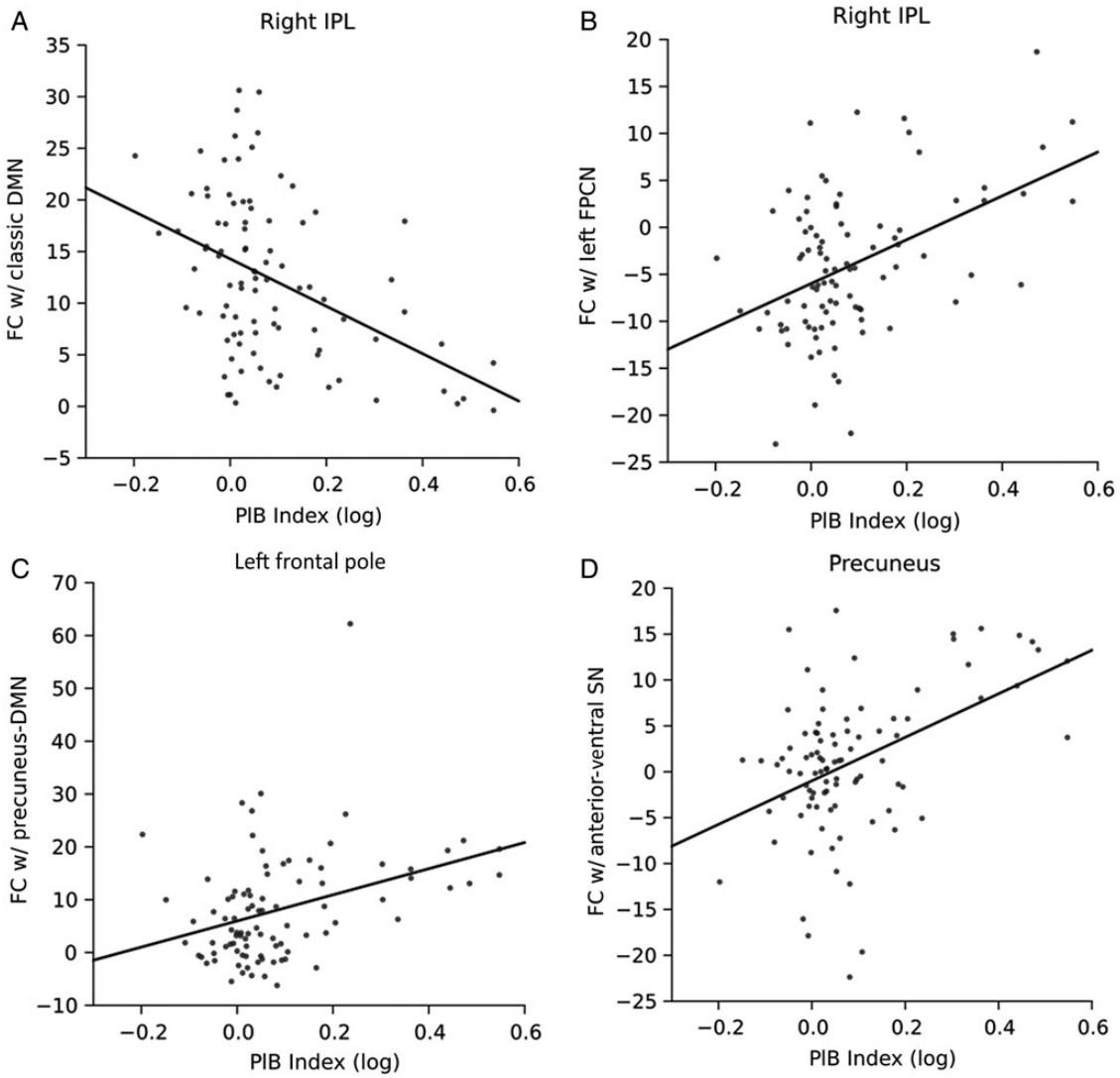

Figure 3. Global PIB ROI examples. Group effects may appear as positive or negative changes in FC related to PIB. However, these effects may be driven by different patterns of connectivity relative to baseline. Parameter estimates generated by dual-regression stage 2 were extracted from significant clusters and plotted against PIB Index (log). Y-axis represents the degree to which the time course of a given region (identified in plot title) is associated with the overall time course of a network (identified in y-axis label). Four examples are shown above: (*A*) The right inferior parietal lobe (IPL) shows a decrease of positive within-network connectivity with the mean network time course of the DMN as PIB increases. (*B*) An increase of between-network connectivity related to PIB that is driven by reduced anti-correlation in the right IPL with the left FPCN. (*C*) An increase in positive connectivity between the left frontal pole and precuneus/DMN time course, which are not strongly coactive at low levels of PIB. (*D*) A flip from anti-correlation between the precuneus and the mean network time course of the anterior–ventral SN at low levels of PIB that becomes positively correlated at high levels.

connectivity, and in fact, these networks tended to be anti-correlated in individuals with low levels of PIB. The increased FC between a region with a time course typical of the right FPCN and the overall left FPCN time course was actually driven by reduced anti-correlation (Fig. 3B). That is, what may have been a competitive balance became less coordinated. Within the precuneus, a region strongly associated with the DMN, we found a shift from negative to positive FC with the anterior–ventral SN (Fig. 3D). This may indicate a more fundamental shift in the way these networks interact rather than a simple alteration in connection strength.

Regional PIB Results

The regional analysis investigated changes of FC related to PIB on a voxelwise basis (Fig. 4 and Table 3). Similar to the global analysis, as regional PIB increased, a cluster of reduced within-network FC to the DMN was apparent in DMN-associated voxels in the right IPL, but extending into regions more commonly associated with the right FPCN. Additionally, there was greater between-network anti-correlation between a part of the left TPJ, which tended to be coactive with the posterior–dorsal SN, and the mean time course or the classic DMN (Fig. 4A). Several posterior brain regions demonstrated reduced anti-correlation with the precuneus/DMN, including the right lateral occipital cortex (LOC) and IPL (falling within regions associated with the DAN, classic DMN, and right FPCN), and the left LOC (more closely related to the DAN) (Fig. 4B). An area in the left frontal pole with a time course more typical of the classic DMN did show increased FC with the precuneus/DMN with heightened regional PIB. There were several parts of the DAN in which within-network FC decreased, including bilateral LOC and superior parietal lobe (Fig. 4C). However, a more inferior portion of the left LOC showed increased FC with the overall network time course. A between-network decrease in FC with the DAN time course was also apparent in the right IPL, which is associated with the classic DMN. As in the global PIB analysis, the left FPCN showed reduced anti-correlation with a region related to the right FPCN, centered in the right SMG (Fig. 4D). However, there was also a within-network increase found in the left frontal pole. A broad swath of cortical regions associated with the right FPCN displayed decreased within-network FC, including the right SMG and right frontal pole (Fig. 4E). In contrast, multiple regions with time courses typical of the posterior–dorsal SN, such as left insular cortex, PFC, and TPJ, became more anti-correlated with the right FPCN (Fig. 4F). The anterior–ventral SN showed both PIB-related increases and decreases across frontal and posterior cortex. A region with a time course more typical of the right FPCN located in the right superior PFC became more correlated with the anterior–ventral SN, whereas the precuneus (associated with the DMN) and right LOC (associated with the posterior–dorsal SN) exhibited decreased anti-correlation. Finally, the insular cortex (associated with the anterior–ventral SN) and fusiform gyrus (associated with the DAN) showed decreased FC with greater amounts of regional PIB.

Discussion

These results demonstrate that changes in FC are not limited to connectivity within the DMN in cognitively normal elderly

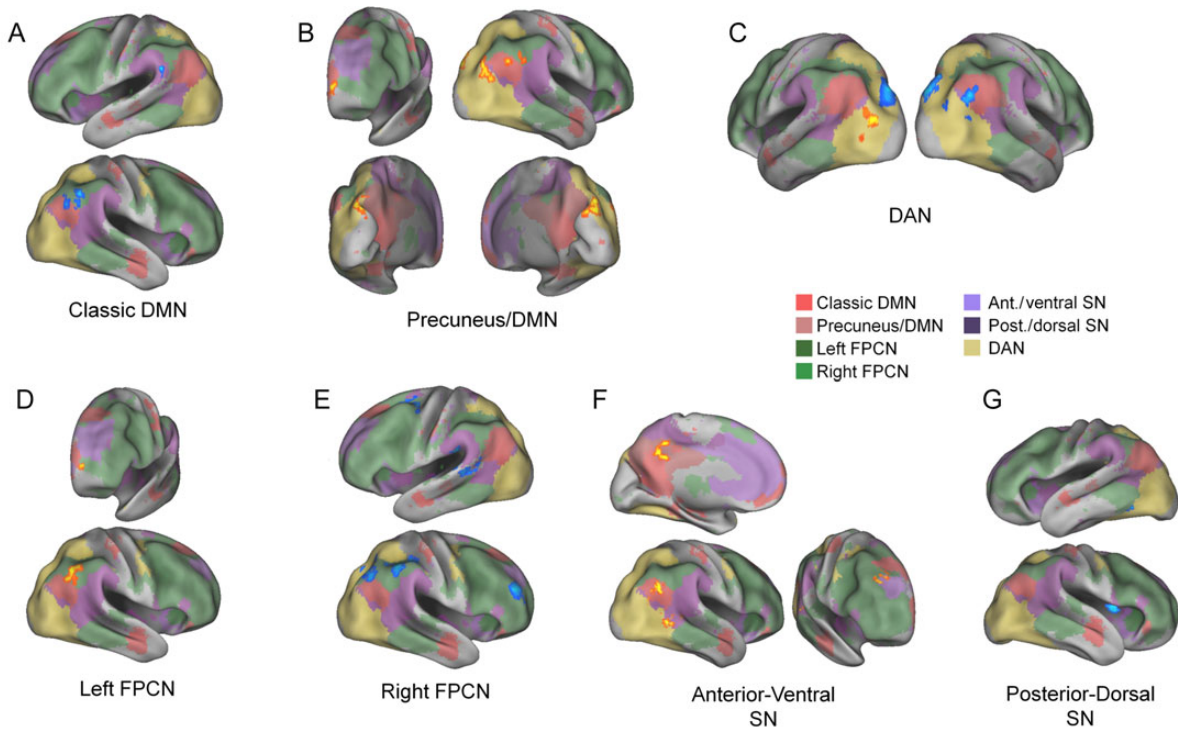

Figure 4. Regional PIB results. Networks showing significant changes in FC related to voxelwise PIB are displayed on inflated surfaces. Statistical maps representing how strongly each voxel's time course was associated with the mean time course of a given network were regressed against each subject's DVR map using a robust regression with the bisquare weight function. Regressors controlling for age, scanner, motion, and voxelwise gray matter were included. Results were cluster-corrected to $P < 0.05$ using a voxel threshold of $P < 0.01$. Each panel displays Aβ-related changes in FC related to a different network time course (identified by the label under each set of brains). Warm colors indicate a positive relationship between voxelwise PIB and the degree of coactivation with the mean network time course; cool colors indicate a negative relationship. See the text for information on directionality relative to baseline. The overlay colors on the brain show the group component with the highest *z*-score for each voxel to demonstrate the network most strongly associated with each region.

Table 3 Local maxima of regional PIB analysis

Region	Hemisphere	Within/outside network[a]	X (mm)	Y (mm)	Z (mm)	z-score
Classic DMN						
Angular gyrus	R	W,O	48	−52	30	−5.89
Supramarginal gyrus	L	O	−62	−48	24	−4.54
Precuneus/DMN						
Angular gyrus	R	W,O	48	−56	28	4.51
Cuneal cortex	R	O	2	−88	40	5.41
Frontal pole	L	W	−16	70	0	3.88
LOC (superior)	L	O	−20	−86	36	4.4
DAN						
LOC (superior)	R	W	22	−86	36	−3.97
	R	W,O	48	−68	30	−3.77
	L	W	−54	−70	22	4.87
	L	W	−18	−86	36	−5.11
Left FPCN						
Angular gyrus	R	O	50	−54	40	5.26
Frontal pole	L	W	−24	66	2	4.52
Right FPCN						
Frontal pole	R	W	40	44	22	−4.41
Insular cortex	L	O	−40	−10	−14	−3.7
LOC (superior)	R	W,O	38	−68	44	−4.02
Occipital Pole	L	O	−40	−94	−4	−5.44
Planum temporale	L	O	−54	−28	10	−4.81
Superior frontal gyrus	L	O	−24	4	54	−3.49
Supramarginal gyrus	R	W	46	−44	46	5.91
Anterior–ventral salience network						
Frontal pole	R	O	32	44	42	4.08
LOC (superior)	R	O	54	−64	28	5.6
Middle temporal gyrus	R	O	54	−56	2	3.72
Precuneus	L	O	−12	−54	34	4.77
Posterior–dorsal salience network						
Insular cortex	R	O	32	2	8	−3.8
Temporal occipital fusiform gyrus	L	O	−40	−52	−14	−3.45

Regions demonstrating changes in FC related to voxelwise PIB DVR are listed for each network. Coordinates of local maxima within significant clusters ($P < 0.05$, cluster-corrected) are reported in MNI-space, and regional labels were derived from the Harvard-Oxford Cortical Atlas. The location of significant clusters is indicated as within or outside a tested network, corresponding to within- or between-network changes of FC, respectively.

[a]W = cluster located within tested network; O = cluster located outside tested network.

subjects harboring Aβ burden. Furthermore, by examining FC on a voxelwise basis, we were able to find effects that occurred in a regionally specific manner rather than across entire networks. This indicates that sub-regions within a network are affected to varying degrees and may possess differential connectivity with the rest of the brain. In addition to these within-network changes, we also found many instances in which regions outside of a given network became more or less correlated with its time course as Aβ increases. This demonstrates that not only do different functional networks possess connections to each other but that these between-network connections are subject to Aβ-related alteration.

Consistent with previous studies, we found disrupted FC within the classic DMN component related to both global and regional PIB (Figs 1A and 3A) (Hedden et al. 2009; Sheline et al. 2010; Mormino, Smiljic, et al. 2011). This finding likely represents dysfunction due to local deposition, as the DMN is 1 of the first networks to accumulate significant Aβ loads and the right angular gyrus is particularly targeted by AD-related effects (Seeley et al. 2009). However, the DMN was not the only network to exhibit altered FC. There was decreased FC in the right FPCN (Figs 2E and 4E) and DAN (Fig. 4C). These clusters were located within association cortex and tended to be adjacent to DMN regions. Amyloid accumulation occurs throughout the association cortex (Buckner et al. 2008); therefore, it is plausible that similar mechanisms underlie effects in the DMN and part of other networks where deposition is especially high. In using a voxelwise approach, we are able to detect localized effects in multiple networks that may not be apparent when assessing FC with summary measures. Together with extant findings that networks are composed of heterogeneous sub-modules (He et al. 2009; Meunier et al. 2009), this suggests that functional reorganization should be examined with units of resolution small enough to allow for a large degree of within-network variability.

Interestingly, PIB-related changes in FC also occurred outside of the networks being assessed, which likely reflect alterations of internetwork connectivity. A cluster in the anterior PFC demonstrated stronger correlation with the mean precuneus/DMN time course at higher levels of PIB (Fig. 2B). A number of studies investigating preclinical and early-stage AD subjects have reported similar FC increases in network connectivity with the DMN among voxels in the anterior PFC (Jones et al. 2011; Mormino, Smiljic, et al. 2011; Damoiseaux et al. 2012). This region of the PFC exhibited a time course more typical of the left FPCN yet its coactivation with the mean DMN time course was altered; thus, it may maintain dual allegiance akin to the connector hubs

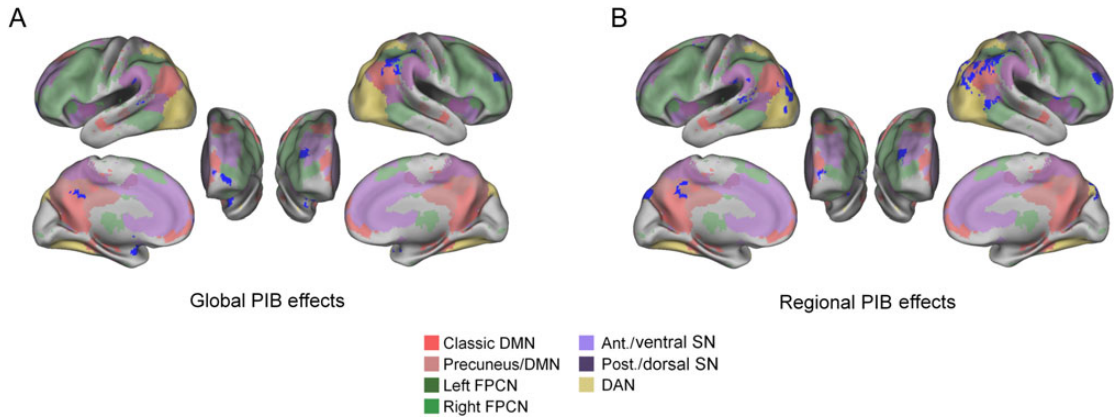

Figure 5. Regions of PIB-related changes in FC. Regions demonstrating a change in FC (either positive or negative) with any network are displayed on inflated brain surfaces. The overlay colors on the brain show the group component with the highest z-score for each voxel to demonstrate the network most strongly associated with each region. The majority of effects occur in medial and lateral parietal cortices and the PFC. The analyses are largely consistent, with a greater extent of changes detected in the regional PIB analysis. However, changes of connectivity in the OFC were only found in the global analysis. These alterations in FC primarily occur in regions where multiple networks converge, and the effects extend across network borders.

described in graph theory (Bullmore and Sporns 2009). In flexibly coupling with other networks, these connectors may have time courses that resemble those of multiple networks. By using a dual regression approach, we were able to measure the degree of coactivation between a voxel with multiple networks simultaneously. The picture that emerges is one in which the FC of multiple networks is affected, both within networks themselves and outside network boundaries. Figure 5 is a map of Aβ-related changes of FC in either direction (increases or decreases) to give a better sense of the cortical regions most affected. Several findings become apparent when viewing the data in this fashion.

Altered FC is most apparent in medial and lateral parietal cortices as well as the anterior PFC and parts of temporal neocortex. While a cursory examination may place these effects generally within the DMN, they in fact extend across regions closely associated with multiple networks, particularly the DAN and FPCN. The sites in which connectivity changes are localized may be more properly characterized as the anatomical and topological "borderlands" between networks. Multiple neural populations with dissociable functional properties come together in the parietal and prefrontal cortices (Gilbert et al. 2006; Nelson et al. 2010). These regions constitute large areas of the association cortex, wherein varied sensory inputs are integrated. Large numbers of intra- and inter-network hubs that underpin information transfer throughout the brain are located here (Buckner et al. 2009; He et al. 2009; Meunier et al. 2009). Additionally, these sites correspond to "zones of instability," or regions that display high-amplitude fluctuations of connectivity with other networks over time (Allen et al. 2014; Hutchison et al. 2013; Jones et al. 2012). It may be that these connections are especially susceptible to failure because the tradeoff for greater flexibility is a degree of instability or weaker connections that are more prone to pathology-induced failure. These regions also overlap with brain regions comprising the "rich club" (Collin et al. 2014; Crossley et al. 2014) that demonstrate aerobic glycolysis (Vaishnavi et al. 2010; Vlassenko et al. 2010), high metabolic demand, and neural plasticity. Metabolic requirements have been proposed as a factor that may be related to the selective vulnerability of these regions to deposition of Aβ (Jagust and Mormino 2011) whereas plasticity has been proposed to underlie regional predilection to neurofibrillary pathology (Mesulam 1999).Support for these ideas comes from a recent report that more Aβ accumulates within canonical resting-state networks in areas of higher network connectivity (Myers et al. 2014). It is also worth noting that although the regional changes in FC seen in Figure 5 were detected in normal older people, they strongly reflect the well-known patterns of regional reductions in glucose metabolism seen in patients with AD (Alexander et al. 2002; Langbaum et al. 2009). These findings suggest reductions in glucose metabolism may be the end stage of neural systems that begin to fail many years before the onset of frank disease.

Some of the effects seen here may be driven by impaired functioning of networks responsible for modulating global activity and coordination rather than dysfunction in local circuits. Large extents of FC loss (and diminished anti-correlation) with the right and left FPCN suggest that these networks are functionally impaired (Figs 1D and 3D). Widespread disruption of these networks may be responsible for some of the changes apparent in other networks. A primary role of the FPCN is to flexibly couple with the DMN and DAN to mediate cross-network communication and facilitate goal-directed behavior (Spreng et al. 2010, 2012; Cole et al. 2013). A lack of inhibitory control brought about by FPCN disconnection has been proposed to underlie the lack of normal suppression in the DMN during task execution (Spreng and Schacter 2012). In a related manner, attenuated anti-correlation between the mean DMN time course and regions with time courses more typical of the DAN may also be driven by a lack of efficient mediation by the FPCN. A similar breakdown in modulatory control may arise in the SN. This network is responsible for detecting salient external stimuli, providing access to attentional resources, and mediating switching between networks (Menon and Uddin 2010). In healthy individuals, there is a dynamic balance between the SN and DMN, such that they may be anti-correlated (Fox et al. 2005; Sridharan et al. 2008). In our data, regions within the medial and lateral posterior parietal cortex closely associated with the DMN showed a positive relationship between FC and PIB driven by a loss of anti-correlation with the mean anterior–ventral SN time course (Figs 2F and 4F). Increased SN connectivity is commonly found among those with MCI, AD, and individuals at genetic risk for AD (Zhou et al. 2010; Machulda et al. 2011; Agosta et al. 2012; Brier et al. 2012; Balthazar et al. 2014; Goveas et al. 2013). While the exact nature of this increased SN connectivity is unclear, 1 possibility is that diminished inhibitory control drives the commonly reported lack

of task-related DMN suppression associated with Aβ (Sperling et al. 2009). Thus, what may appear as decreased FC due to local dysfunction in studies focused on individual networks may in fact be downstream effects precipitated by control network inefficiencies.

It is likely that the changes reported here reflect a mix of deleterious processes as well as compensatory mechanisms that facilitate normal cognitive performance despite the presence of Aβ pathology. The left anterior PFC showed increased FC (Figs 2B, 4B and D) similar to those reported in preclinical AD (Mormino et al. 2012), MCI, and early AD (Qi et al. 2010; Jones et al. 2011; Damoiseaux et al. 2012). In the aging literature, heightened anterior frontal engagement, particularly in the left hemisphere, is taken to reflect compensatory reorganization, as it is associated with higher performance in older adults (Cabeza et al. 2002; Morcom 2003; Rajah and D'Esposito 2005). Increased frontal connectivity during the resting state has been proposed to reflect changes to the underlying network structure which manifests as activity increases during task execution (Qi et al. 2010; Damoiseaux et al. 2012). Although the PFC is the site of significant Aβ burden, it appears to be relatively spared from degeneration and maintains the longest delay before functional abnormalities become apparent (Jack et al. 2008, 2010). Furthermore, a study by Damoiseaux et al. (2012) found that regions exhibiting increased connectivity in AD patients compared with controls tended to show decreases over time. Likewise, the SN demonstrates a similar pattern of increased connectivity during early disease states, which progressively declines during later stages. This suggests a compensatory response that ultimately fails in the face of overwhelming pathology (Brier et al. 2012). Areas of higher PIB-related FC also occurred in posterior cortex, particularly in the LOC. It is possible that these effects represent a compensatory engagement of the visual system as suggested in the previous rs-fMRI and task-based studies (Sheline et al. 2010; Mormino et al. 2012). Thus, although the task-related and resting-state findings do not necessary reflect identical phenomena, these alterations may reflect a compensatory response that is engaged during aging and the initial deposition of Aβ, which contributes to the intact cognitive abilities in high PIB individuals.

Some limitations of the current study should be noted. First, due to the cross-sectional nature of the study, we are not able to determine how alterations of FC evolve over time. To the extent that amyloid accumulation induces similar effects across people, the amount of PIB binding may serve as a proxy for disease staging and provide insight into the progression of neural response. However, longitudinal studies are needed to accurately assess the impact of individual differences and factors such as cognitive reserve on this process. Second, when clusters of Aβ-related alterations in FC fall in a region outside the borders of a given network, we have identified which other network the region's time course is most typical of. We propose that these areas may maintain dual allegiance with multiple networks, but more targeted studies are needed to definitively identify the networks affected by changes in cross-network connectivity. Third, although we have attempted to match the level of smoothing between images of different modalities, the differences in inherent spatial resolution of the fMRI and PIB-PET images may limit the spatial specificity of our results. However, we believe that even a low-resolution PIB-PET image provides a more nuanced measure of regional variability with which to compare changes in FC compared with a global measure such as PIB Index.

The present study provides evidence for widespread network reorganization associated with Aβ deposition. Changes in FC associated with Aβ occur both within and between ICNs and are not limited to the DMN but rather occur in brain regions that demonstrate selective vulnerability that may be related to metabolic and plastic requirements of heteromodal association cortex. Some of these changes most likely represent deleterious effects brought on by Aβ. This may arise from local neural dysfunction, or more indirectly, from disrupted modulatory function of control networks. However, the fact that these changes occur in individuals who remain cognitively normal suggests that some of the changes reported here could also reflect compensatory network reorganization. A more targeted investigation of the behavioral consequences related to changes over time will be necessary to delineate these possibilities. If Aβ deposition is considered a marker of preclinical AD, assessing the extent of reorganization within multiple ICNs may serve as a useful biomarker of disease progression and the brain's response to it.

Funding

This work was supported by NIH grant AG034570.

References

Abou-Elseoud A, Starck T, Remes J, Nikkinen J, Tervonen O, Kiviniemi V. 2010. The effect of model order selection in group PICA. Hum Brain Mapp. 31:1207–1216.

Agosta F, Pievani M, Geroldi C, Copetti M, Frisoni GB, Filippi M. 2012. Resting state fMRI in Alzheimer's disease: beyond the default mode network. Neurobiol Aging. 33:1564–1578.

Agosta F, Vossel KA, Miller BL, Migliaccio R, Bonasera SJ, Filippi M, Boxer AL, Karydas A, Possin KL, Gorno-Tempini ML. 2009. Apolipoprotein E ε4 is associated with disease-specific effects on brain atrophy in Alzheimer's disease and frontotemporal dementia. Proc Natl Acad Sci. 106:2018–2022.

Aizenstein HJ, Nebes RD, Saxton JA, Price JC, Mathis CA, Tsopelas ND, Ziolko SK, James JA, Snitz BE, Houck PR, others. 2008. Frequent amyloid deposition without significant cognitive impairment among the elderly. Arch Neurol. 65:1509.

Alexander GE, Chen K, Pietrini P, Rapoport SI, Reiman EM. 2002. Longitudinal PET evaluation of cerebral metabolic decline in dementia: a potential outcome measure in Alzheimer's disease treatment studies. Am J Psychiatry. 159:738–745.

Allen EA, Damaraju E, Plis SM, Erhardt EB, Eichele T, Calhoun VD. 2014. Tracking whole-brain connectivity dynamics in the resting state. Cereb Cortex. 24:663–676.

Balthazar MLF, Pereira FRS, Lopes TM, da Silva EL, Coan AC, Campos BM, Duncan NW, Stella F, Northoff G, Damasceno BP, et al. 2014. Neuropsychiatric symptoms in Alzheimer's disease are related to functional connectivity alterations in the salience network. Hum Brain Mapp. 35:1237–1246.

Beckmann CF. 2012. Modelling with independent components. NeuroImage. 62:891–901.

Beckmann CF, DeLuca M, Devlin JT, Smith SM. 2005. Investigations into resting-state connectivity using independent component analysis. Philos Trans R Soc B Biol Sci. 360:1001–1013.

Beckmann CF, Mackay CE, Filippini N, Smith SM. 2009. Group comparison of resting-state FMRI data using multi-subject ICA and dual regression. Neuroimage. 47:S148.

Bennett DA, Schneider JA, Arvanitakis Z, Kelly JF, Aggarwal NT, Shah RC, Wilson RS. 2006. Neuropathology of older persons without cognitive impairment from two community-based studies. Neurology. 66:1837–1844.

Binnewijzend MAA, Schoonheim MM, Sanz-Arigita E, Wink AM, van der Flier WM, Tolboom N, Adriaanse SM, Damoiseaux JS,

Scheltens P, van Berckel BNM, et al. 2012. Resting-state fMRI changes in Alzheimer's disease and mild cognitive impairment. Neurobiol Aging. 33:2018–2028.
Biswal B, Zerrin Yetkin F, Haughton VM, Hyde JS. 1995. Functional connectivity in the motor cortex of resting human brain using echo-planar MRI. Magn Reson Med. 34:537–541.
Braak H, Braak E. 1991. Neuropathological stageing of Alzheimer-related changes. Acta Neuropathol (Berl). 82:239–259.
Brier MR, Thomas JB, Snyder AZ, Benzinger TL, Zhang D, Raichle ME, Holtzman DM, Morris JC, Ances BM. 2012. Loss of intranetwork and internetwork resting state functional connections with Alzheimer's disease progression. J Neurosci. 32:8890–8899.
Buckner RL. 2004. Memory and executive function in aging and AD: multiple factors that cause decline and reserve factors that compensate. Neuron. 44:195–208.
Buckner RL. 2005. Molecular, structural, and functional characterization of Alzheimer's disease: evidence for a relationship between default activity, amyloid, and memory. J Neurosci. 25:7709–7717.
Buckner RL, Andrews-Hanna JR, Schacter DL. 2008. The brain's default network: anatomy, function, and relevance to disease. Ann N Y Acad Sci. 1124:1–38.
Buckner RL, Sepulcre J, Talukdar T, Krienen FM, Liu H, Hedden T, Andrews-Hanna JR, Sperling RA, Johnson KA. 2009. Cortical hubs revealed by intrinsic functional connectivity: mapping, assessment of stability, and relation to Alzheimer's disease. J Neurosci. 29:1860–1873.
Bullmore E, Sporns O. 2009. Complex brain networks: graph theoretical analysis of structural and functional systems. Nat Rev Neurosci. 10:186–198.
Cabeza R, Anderson ND, Locantore JK, McIntosh AR. 2002. Aging gracefully: compensatory brain activity in high-performing older adults. NeuroImage. 17:1394–1402.
Casanova R, Ryali S, Baer A, Laurienti PJ, Burdette JH, Hayasaka S, Flowers L, Wood F, Maldjian JA. 2007. Biological parametric mapping: a statistical toolbox for multi-modality brain image analysis. NeuroImage. 34:137–143.
Cole MW, Reynolds JR, Power JD, Repovs G, Anticevic A, Braver TS. 2013. Multi-task connectivity reveals flexible hubs for adaptive task control. Nat Neurosci. 16:1348–1355.
Collin G, Sporns O, Mandl RCW, van den Heuvel MP. 2014. Structural and functional aspects relating to cost and benefit of rich club organization in the human cerebral cortex. Cereb Cortex. 24:2258–2267.
Crossley NA, Mechelli A, Scott J, Carletti F, Fox PT, McGuire P, Bullmore ET. 2014. The hubs of the human connectome are generally implicated in the anatomy of brain disorders. Brain. 137:2382–2395.
Dale AM, Fischl B, Sereno MI. 1999. Cortical surface-based analysis: I. Segmentation and surface reconstruction. NeuroImage. 9:179–194.
Damoiseaux JS, Prater KE, Miller BL, Greicius MD. 2012. Functional connectivity tracks clinical deterioration in Alzheimer's disease. Neurobiol Aging. 33:828.e19–828.e30.
Damoiseaux JS, Rombouts SARB, Barkhof F, Scheltens P, Stam CJ, Smith SM, Beckmann CF. 2006. Consistent resting-state networks across healthy subjects. Proc Natl Acad Sci USA. 103:13848–13853.
Davis DG, Schmitt FA, Wekstein DR, Markesbery WR. 1999. Alzheimer neuropathologic alterations in aged cognitively normal subjects. J Neuropathol Exp Neurol. 58:376–388.
Delis DC, Kramer JH, Kaplan E, Ober BA. 2000. California Verbal Learning Test, 2nd ed. San Antonia, TX: Psychological Corporation.
Dickson DW, Crystal HA, Mattiace LA, Masur DM, Blau AD, Davies P, Yen S-H, Aronson MK. 1992. Identification of normal and pathological aging in prospectively studied nondemented elderly humans. Neurobiol Aging. 13:179–189.
Filippini N, MacIntosh BJ, Hough MG, Goodwin GM, Frisoni GB, Smith SM, Matthews PM, Beckmann CF, Mackay CE. 2009. Distinct patterns of brain activity in young carriers of the APOE-ε4 allele. Proc Natl Acad Sci. 106:7209–7214.
Fox MD, Snyder AZ, Vincent JL, Corbetta M, Essen DCV, Raichle ME. 2005. The human brain is intrinsically organized into dynamic, anticorrelated functional networks. Proc Natl Acad Sci USA. 102:9673–9678.
Friston KJ, Penny WD, Ashburner J, Kiebel SJ, Nichols TE. 2006. Statistical Parametric Mapping: the Analysis of Functional Brain Images. London: Academic Press.
Gilbert SJ, Spengler S, Simons JS, Steele JD, Lawrie SM, Frith CD, Burgess PW. 2006. Functional specialization within rostral prefrontal cortex (area 10): a meta-analysis. J Cogn Neurosci. 18:932–948.
Goveas JS, Xie C, Chen G, Li W, Ward BD, Franczak MB, Jones JL, Antuono PG, Li S-J. 2013. Functional network endophenotypes unravel the effects of apolipoprotein E Epsilon 4 in middle-aged adults. PLoS ONE. 8:e55902.
Greicius MD, Krasnow B, Reiss AL, Menon V. 2003. Functional connectivity in the resting brain: a network analysis of the default mode hypothesis. Proc Natl Acad Sci. 100:253–258.
Greicius MD, Srivastava G, Reiss AL, Menon V. 2004. Default-mode network activity distinguishes Alzheimer's disease from healthy aging: evidence from functional MRI. Proc Natl Acad Sci USA. 101:4637–4642.
Hardy J, Selkoe DJ. 2002. The amyloid hypothesis of Alzheimer's disease: progress and problems on the road to therapeutics. Science. 297:353–356.
He X, Qin W, Liu Y, Zhang X, Duan Y, Song J, Li K, Jiang T, Yu C. 2014. Abnormal salience network in normal aging and in amnestic mild cognitive impairment and Alzheimer's disease. Hum Brain Mapp. 35:3446–3464.
He Y, Wang J, Wang L, Chen ZJ, Yan C, Yang H, Tang H, Zhu C, Gong Q, Zang Y, et al. 2009. Uncovering intrinsic modular organization of spontaneous brain activity in humans. PLoS ONE. 4:1932–6203.
Hedden T, Van Dijk KR, Becker JA, Mehta A, Sperling RA, Johnson KA, Buckner RL. 2009. Disruption of functional connectivity in clinically normal older adults harboring amyloid burden. J Neurosci. 29:12686.
Hulette CM, Welsh-Bohmer KA, Murray MG, Saunders AM, Mash DC, McIntyre LM. 1998. Neuropathological and neuropsychological changes in "normal" aging: evidence for preclinical Alzheimer disease in cognitively normal individuals. J Neuropathol Exp Neurol. 57:1168–1174.
Hutchison RM, Womelsdorf T, Gati JS, Everling S, Menon RS. 2013. Resting-state networks show dynamic functional connectivity in awake humans and anesthetized macaques. Hum Brain Mapp. 34:2154–2177.
Jack CR, Knopman DS, Jagust WJ, Petersen RC, Weiner MW, Aisen PS, Shaw LM, Vemuri P, Wiste HJ, Weigand SD, et al. 2013. Tracking pathophysiological processes in Alzheimer's disease: an updated hypothetical model of dynamic biomarkers. Lancet Neurol. 12:207–216.

Jack CR, Lowe VJ, Senjem ML, Weigand SD, Kemp BJ, Shiung MM, Knopman DS, Boeve BF, Klunk WE, Mathis CA, et al. 2008. 11C PiB and structural MRI provide complementary information in imaging of Alzheimer's disease and amnestic mild cognitive impairment. Brain. 131:665–680.

Jack CR, Wiste HJ, Vemuri P, Weigand SD, Senjem ML, Zeng G, Bernstein MA, Gunter JL, Pankratz VS, Aisen PS, et al., the Alzheimer's Disease Neuroimaging Initiative. 2010. Brain beta-amyloid measures and magnetic resonance imaging atrophy both predict time-to-progression from mild cognitive impairment to Alzheimer's disease. Brain. 133: 3336–3348.

Jagust WJ, Mormino EC. 2011. Lifespan brain activity, β-amyloid, and Alzheimer's disease. Trends Cogn Sci. 15:520–526.

Jones DT, Machulda MM, Vemuri P, McDade EM, Zeng G, Senjem ML, Gunter JL, Przybelski SA, Avula RT, Knopman DS, et al. 2011. Age-related changes in the default mode network are more advanced in Alzheimer disease. Neurology. 77:1524–1531.

Jones DT, Vemuri P, Murphy MC, Gunter JL, Senjem ML, Machulda MM, Przybelski SA, Gregg BE, Kantarci K, Knopman DS, et al. 2012. Non-stationarity in the "resting brain's" modular architecture. PLoS ONE. 7:e39731.

Klunk WE, Engler H, Nordberg A, Wang Y, Blomqvist G, Holt DP, Bergström M, Savitcheva I, Huang G-F, Estrada S, et al. 2004. Imaging brain amyloid in Alzheimer's disease with Pittsburgh Compound-B. Ann Neurol. 55:306–319.

Knopman DS, Parisi JE, Salviati A, Floriach-Robert M, Boeve BF, Ivnik RJ, Smith GE, Dickson DW, Johnson KA, Petersen LE, et al. 2003. Neuropathology of cognitively normal elderly. J Neuropathol Exp Neurol. 62:1087–1095.

Laird AR, Fox PM, Eickhoff SB, Turner JA, Ray KL, McKay DR, Glahn DC, Beckmann CF, Smith SM, Fox PT. 2011. Behavioral interpretations of intrinsic connectivity networks. J Cogn Neurosci. 23:4022–4037.

Langbaum JBS, Chen K, Lee W, Reschke C, Bandy D, Fleisher AS, Alexander GE, Foster NL, Weiner MW, Koeppe RA, et al. 2009. Categorical and correlational analyses of baseline fluorodeoxyglucose positron emission tomography images from the Alzheimer's disease neuroimaging initiative (ADNI). NeuroImage. 45:1107–1116.

Logan J, Fowler JS, Volkow ND, Wang G-J, Ding Y-S, Alexoff DL. 1996. Distribution volume ratios without blood sampling from graphical analysis of PET data. J Cereb Blood Flow Metab. 16:834–840.

Machulda MM, Jones DT, Vemuri P, McDade E, Avula R, Przybelski S, Boeve BF, Knopman DS, Petersen RC, Jack CR. 2011. Effect of apoe ε4 status on intrinsic network connectivity in cognitively normal elderly. Arch Neurol. 68: 1131–1136.

Menon V, Uddin LQ. 2010. Saliency, switching, attention and control: a network model of insula function. Brain Struct Funct. 214:655–667.

Mesulam MM. 1999. Neuroplasticity failure in Alzheimer's disease: bridging the gap between plaques and tangles. Neuron. 24:521–529.

Meunier D, Lambiotte R, Fornito A, Ersche K, Bullmore ET, Meunier D, Lambiotte R, Fornito A, Ersche KD, Bullmore ET. 2009. Hierarchical modularity in human brain functional networks. Front Neuroinformatics. 3:37.

Morcom AM. 2003. Age effects on the neural correlates of successful memory encoding. Brain. 126:213–229.

Mormino EC, Brandel MG, Madison CM, Marks S, Baker SL, Jagust WJ. 2012. Aβ Deposition in aging is associated with increases in brain activation during successful memory encoding. Cereb Cortex. 22:1813–1823.

Mormino EC, Smiljic A, Hayenga AO, Onami SH, Greicius MD, Rabinovici GD, Janabi M, Baker SL, Yen IV, Madison CM, et al. 2011. Relationships between beta-amyloid and functional connectivity in different components of the default mode network in aging. Cereb Cortex. 21:2399–2407.

Morris JC, Roe CM, Xiong C, Fagan AM, Goate AM, Holtzman DM, Mintun MA. 2010. APOE predicts amyloid-beta but not tau Alzheimer pathology in cognitively normal aging. Ann Neurol. 67:122–131.

Myers N, Pasquini L, Göttler J, Grimmer T, Koch K, Ortner M, Neitzel J, Mühlau M, Fürster S, Kurz A, et al. 2014. Within-patient correspondence of amyloid-β and intrinsic network connectivity in Alzheimer's disease. Brain J Neurol. 137: 2052–2064.

Nelson SM, Cohen AL, Power JD, Wig GS, Miezin FM, Wheeler ME, Velanova K, Donaldson DI, Phillips JS, Schlaggar BL. 2010. A parcellation scheme for human left lateral parietal cortex. Neuron. 67:156–170.

Oh H, Habeck C, Madison C, Jagust W. 2014. Covarying alterations in Aβ deposition, glucose metabolism, and gray matter volume in cognitively normal elderly. Hum Brain Mapp. 35:297–308.

Price JC, Klunk WE, Lopresti BJ, Lu X, Hoge JA, Ziolko SK, Holt DP, Meltzer CC, DeKosky ST, Mathis CA. 2005. Kinetic modeling of amyloid binding in humans using PET imaging and Pittsburgh Compound-B. J Cereb Blood Flow Metab. 25: 1528–1547.

Price JL, McKeel DW Jr., Buckles VD, Roe CM, Xiong C, Grundman M, Hansen LA, Petersen RC, Parisi JE, Dickson DW, et al. 2009. Neuropathology of nondemented aging: presumptive evidence for preclinical Alzheimer disease. Neurobiol Aging. 30: 1026–1036.

Qi Z, Wu X, Wang Z, Zhang N, Dong H, Yao L, Li K. 2010. Impairment and compensation coexist in amnestic MCI default mode network. NeuroImage. 50:48–55.

Rabinovici GD, Furst AJ, O'Neil JP, Racine CA, Mormino EC, Baker SL, Chetty S, Patel P, Pagliaro TA, Klunk WE, et al. 2007. 11C-PIB PET imaging in Alzheimer disease and frontotemporal lobar degeneration. Neurology. 68: 1205–1212.

Raichle ME, MacLeod AM, Snyder AZ, Powers WJ, Gusnard DA, Shulman GL. 2001. A default mode of brain function. Proc Natl Acad Sci. 98:676–682.

Rajah MN, D'Esposito M. 2005. Region-specific changes in prefrontal function with age: a review of PET and fMRI studies on working and episodic memory. Brain. 128: 1964–1983.

Rytty R, Nikkinen J, Paavola L, Abou Elseoud A, Moilanen V, Visuri A, Tervonen O, Renton AE, Traynor BJ, Kiviniemi V, et al. 2013. GroupICA dual regression analysis of resting state networks in a behavioral variant of frontotemporal dementia. Front Hum Neurosci. 7:1662–5161.

Sanz-Arigita EJ, Schoonheim MM, Damoiseaux JS, Rombouts SARB, Maris E, Barkhof F, Scheltens P, Stam CJ. 2010. Loss of "small-world" networks in Alzheimer's disease: graph analysis of fMRI resting-state functional connectivity. PLoS One. 5: e13788.

Seeley WW, Crawford RK, Zhou J, Miller BL, Greicius MD. 2009. Neurodegenerative diseases target large-scale human brain networks. Neuron. 62:42–52.

Sheline YI, Raichle ME, Snyder AZ, Morris JC, Head D, Wang S, Mintun MA. 2010. Amyloid plaques disrupt resting state

default mode network connectivity in cognitively normal elderly. Biol Psychiatry. 67:584–587.

Shirer WR, Ryali S, Rykhlevskaia E, Menon V, Greicius MD. 2012. Decoding subject-driven cognitive states with whole-brain connectivity patterns. Cereb Cortex. 22:158–165.

Smith SM, Jenkinson M, Woolrich MW, Beckmann CF, Behrens TE, Johansen-Berg H, Bannister PR, De Luca M, Drobnjak I, Flitney DE, others. 2004. Advances in functional and structural MR image analysis and implementation as FSL. Neuroimage. 23:208–219.

Sperling RA, LaViolette PS, O'Keefe K, O'Brien J, Rentz DM, Pihlajamaki M, Marshall G, Hyman BT, Selkoe DJ, Hedden T. 2009. Amyloid deposition is associated with impaired default network function in older persons without dementia. Neuron. 63:178–188.

Spreng RN, Schacter DL. 2012. Default network modulation and large-scale network interactivity in healthy young and old adults. Cereb Cortex. 22:2610–2621.

Spreng RN, Sepulcre J, Turner GR, Stevens WD, Schacter DL. 2012. Intrinsic architecture underlying the relations among the default, dorsal attention, and frontoparietal control networks of the human brain. J Cogn Neurosci. 25:74–86.

Spreng RN, Stevens WD, Chamberlain JP, Gilmore AW, Schacter DL. 2010. Default network activity, coupled with the frontoparietal control network, supports goal-directed cognition. NeuroImage. 53:303–317.

Sridharan D, Levitin DJ, Menon V. 2008. A critical role for the right fronto-insular cortex in switching between central-executive and default-mode networks. Proc Natl Acad Sci. 105: 12569–12574.

Stam CJ, Jones BF, Nolte G, Breakspear M, Scheltens P. 2007. Small-world networks and functional connectivity in Alzheimer's disease. Cereb Cortex. 17:92–99.

Supekar K, Menon V, Rubin D, Musen M, Greicius MD. 2008. Network analysis of intrinsic functional brain connectivity in Alzheimer's disease. PLoS Comput Biol. 4:e1000100.

Vaishnavi SN, Vlassenko AG, Rundle MM, Snyder AZ, Mintun MA, Raichle ME. 2010. Regional aerobic glycolysis in the human brain. Proc Natl Acad Sci. 107:17757–17762.

Van Essen DC. 2005. A population-average, landmark-and surface-based (PALS) atlas of human cerebral cortex. NeuroImage. 28:635–662.

Villemagne VL, Burnham S, Bourgeat P, Brown B, Ellis KA, Salvado O, Szoeke C, Macaulay SL, Martins R, Maruff P, et al. 2013. Amyloid β deposition, neurodegeneration, and cognitive decline in sporadic Alzheimer's disease: a prospective cohort study. Lancet Neurol. 12:357–367.

Vlassenko AG, Vaishnavi SN, Couture L, Sacco D, Shannon BJ, Mach RH, Morris JC, Raichle ME, Mintun MA. 2010. Spatial correlation between brain aerobic glycolysis and amyloid-β (Aβ) deposition. Proc Natl Acad Sci. 107:17763–17767.

Walsh DM, Selkoe DJ. 2004. Deciphering the molecular basis of memory failure in Alzheimer's disease. Neuron. 44:181–193.

Wang K, Liang M, Wang L, Tian L, Zhang X, Li K, Jiang T. 2007. Altered functional connectivity in early Alzheimer's disease: a resting-state fMRI study. Hum Brain Mapp. 28:967–978.

Wechsler D. 1997. Wechsler Adult Intelligence Scale-III (WAIS-III) manual. New York: The Psychological Corporation.

Yang X, Beason-Held L, Resnick SM, Landman BA. 2011. Biological parametric mapping with robust and non-parametric statistics. NeuroImage. 57:423–430.

Zhou J, Greicius MD, Gennatas ED, Growdon ME, Jang JY, Rabinovici GD, Kramer JH, Weiner M, Miller BL, Seeley WW. 2010. Divergent network connectivity changes in behavioural variant frontotemporal dementia and Alzheimer's disease. Brain J Neurol. 133:1352–1367.